"Nearly Thresholdless Optical Gain using Colloidal HgTe Nanocrystals "

Pieter Geiregat[1,2,3], Arjan J. Houtepen[4], Ferdinand C. Grozema[4], Laxmi Kishore Sagar[2,3], Guy Allan[5], Christophe Delerue[5], Dries van Thourhout[1,3], Zeger Hens[2,3,*]

[1] Photonics Research Group, University of Ghent, Ghent, Belgium
[2] Physics and Chemistry of Nanostructures group, University of Ghent, Ghent, Belgium
[3]Center for Nano and Biophotonics, University of Ghent, Ghent, Belgium
[4]Opto-Electronic Materials Section, Delft University of Technology, Delft, The Netherlands
[5]IEMN, Département Institut Supérieure d'Electronique et du Numérique, UMR CNRS, Lille, France

* To whom correspondence should be sent: Zeger.Hens@ugent.be

Contact information of authors:

Pieter Geiregat
E-mail: Pieter.Geiregat@Ugent.be
Address: Department of Information Technology, Sint-Pietersnieuwstraat 41, B-9000 Gent, Belgium

Arjan J. Houtepen
E-mail: A.J.Houtepen@tudelft.nl
Address: Opto-electronic Materials Section, Faculty of Applied Sciences, Department of Chemical Engineering, Delft University of Technology, Julianalaan 136, 2628 BL Delft, The Netherlands

Ferdinand C. Grozema
E-mail: F.C.Grozema@tudelft.nl
Address: Opto-electronic Materials Section, Faculty of Applied Sciences, Department of Chemical Engineering, Delft University of Technology, Julianalaan 136, 2628 BL Delft, The Netherlands

Laxmi Kishore Sagar
E-mail: LaxmiKishoreSagar.Chiluka@UGent.be
Address: Department of Inorganic and Physical Chemistry, Krijgslaan 281(S3), B-9000 Gent, Belgium

Guy Allan
E-mail: guy.allan@isen.iemn.univ-lille1.fr
Address: IEMN, Département ISEN, UMR CNRS – 8520, Lille, France

Christophe Delerue
E-mail: Christophe.Delerue@isen.fr
Address: IEMN, Département ISEN, UMR CNRS – 8520, Lille, France

Dries Vanthourhout
E-mail: Dries.Vanthourhout@Ugent.be
Address: Department of Information Technology, Sint-Pietersnieuwstraat 41, B-9000 Gent, Belgium

*Zeger Hens
E-mail: Zeger.Hens@Ugent.be
Address: Department of Inorganic and Physical Chemistry, Krijgslaan 281(S3), B-9000 Gent, Belgium

No prior discussion with Nature Editors made

Submission relevance to Nature:

…

Summary

Articles have a separate summary of up to 150 words, which has no references, and does not contain numbers, abbreviations, acronyms or measurements unless essential. It contains 2–3 sentences of basic-level introduction to the field; a brief account of the background and rationale of the work; a statement of the main conclusions (introduced by the phrase 'Here we show' or its equivalent); and 2–3 sentences putting the main findings into general context so it is clear how the results described have moved the field forwards.

The use of colloidal quantum dots (QDs) as a tunable and solution-processable gain medium for optical amplifiers or lasers is still elusive in spite of 15 years of intense research. Gain thresholds remain too high and gain lifetimes too short for practical purposes. These properties are intrinsically linked to the QDs being effective 2-level systems, where the emitting transition is countered by absorption. Here, we show that HgTe QDs exhibit size-tunable stimulated emission throughout the infrared telecom window at a threshold 2 orders of magnitude lower than ever reported for QDs. We demonstrate that stimulated emission involves a high oscillator strength transition to a gap state, making HgTe QDs a nearly thresholdless effective 3-level system. The combination of gain coefficient, threshold and lifetime makes DC electrical pumping using HgTe QDs a possibility for the first time, a result showing that the formation of effective 3-level systems is a new paradigm for developing QD-based gain media.

Main Text

Articles are typically 3,000 words of text, beginning with up to 500 words of referenced text expanding on the background to the work (some overlap with the summary is acceptable), before proceeding to a concise, focused account of the findings, ending with one or two short paragraphs of discussion. The text may contain a few short subheadings (not more than six in total) of no more than 40 characters each (less than one line of text in length). Articles typically have 5 or 6 display items (figures or tables).

Colloidal quantum dots (QDs) combine size-tuneable electronic energy levels with a suitability for solution-based processing, which makes them ideal for numerous optoelectronic applications[1]. QD photodetectors[2], solar cells[3], white LEDs and

displays[4] all make use of the broad QD absorption spectrum with its size-dependent onset corresponding to the lowest energy exciton (X) or bandgap transition and/or the tunable, narrow emission spectrum resulting from exciton recombination. Application development is further driven by unique characteristics such as multi-X generation[5] or room-temperature single photon emission[6] and the possibility to fine-tune opto-electronic properties by heterostructure formation[7], doping[8] or alloying[9].

Devices relying on optical gain, such as lasers or amplifiers could equally benefit from tunable, low cost and solution processable gain media. Taking the example of the telecom wavelengths around 1.3 and 1.55 μm – used in long haul fibre-based datacommunication and integrated silicon-on-insulator (SOI) photonic circuits for signal processing and sensing[10,11] – lasers are fabricated through expensive vacuum epitaxy of III-V semiconductors. Combining the latter with SOI requires bonding of III-V dies or direct epitaxial growth on silicon. Both suffer from cost, upscaling and efficiency issues, problems not solved by recent direct integration efforts such as erbium doping[12,13] and strained Ge[14], which are limited by gain bandwidth, efficiency and/or cost of fabrication.

Although stimulated emission involving the bandgap transition has been demonstrated for different QDs[15–18],their use as a gain medium has been limited. This is largely due to the QDs being an effective two-level system, where stimulated emission and absorption involve transitions between the same discrete band edge states. Since these are degenerate, QDs must contain more than one exciton on average to achieve population inversion[15]. Next to this intrinsic drawback of two-level gain media, multi-X rapidly recombine through non-radiative Auger processes[19], limiting the gain lifetime to a few tens of picoseconds. Although the resulting high thresholds can be reached by optical pumping using pulsed lasers[20], this makes QD-based gain media of little use, especially in technologically more relevant electrically pumped devices.

Two strategies have been proposed to circumvent the limitations imposed by multi-X gain. It proved possible to slow down Auger recombination through interfacial alloying in core/shell QDs and/or using large volume QDs[21]. Alternatively, single-X gain[16,22] has been demonstrated using so-called type II core/shell QDs, where the spatial separation of electron and hole leads to repulsive X-X interactions, lifting the effective level degeneracy. Unfortunately, both strategies are restricted to a few materials – typically involving Cd-based QDs emitting in the visible – and gain still relies on a two level scheme.

Here, we report on optical gain in dispersions of HgTe QDs with average exciton numbers per nanocrystal $\langle N \rangle$ as low as 0.005. Intrinsic gain coefficients of about 500 cm^{-1} are demonstrated and the extrapolated gain lifetime corresponds to the single exciton radiative lifetime of 34 ns. We attribute this almost thresholdless gain to stimulated emission between the lowest conduction band level and shallow, empty surface states near the first valence band level, thus creating a nearly thresholdless, effective 3-level system. Since the gain characteristics meet the requirements for DC electrical pumping[23], this result shows that the use of effective 3-level systems is the way forward for developing performing QD-based gain media.

(514 words)

Basic properties of HgTe nanocrystals

HgTe is a II-VI compound that stands out since it is a semi-metal with a direct negative bulk band gap. As a result, the HgTe band gap can be tuned from the long-wave infrared down to the near-infrared by means of size quantization, where bandgaps up to 1 eV can be reached with 3 to 4 nm nanocrystals. The colloidal HgTe QDs used here have been synthesized according to a modified literature procedure[24,25] (see Methods). As show in Figure 1a and 1b, this leads to somewhat irregular nanocrystals with the zinc blende crystal structure. The absorption and emission spectra of these HgTe QDs (Figure 1c) feature the typical characteristics of the first exciton transition, albeit with a large apparent Stokes shift (120 meV for the data shown) between emission and absorption. By changing the reaction conditions, the absorption and emission spectrum can be tuned throughout the entire near-infrared spectrum (from 1100 nm to 1600 nm). Time-resolved photoluminescence under low-fluence excitation shows a non-exponential decay, which can be fitted using a double exponential with a short 30-40 ns and a longer 75 ns decay time (see Figure 1d).

Figure 1e represents the upper valence band (low energy side) and lower conduction band (high energy side) electronic states of spherical, 3.5 nm HgTe QDs calculated using a semi-empirical tight binding approach[26](see Methods). Whereas the lowest conduction band level (CB1) is a 2-fold degenerate state well separated from higher levels, two closely spaced, 4-fold degenerate levels (VB1 and VB2) are found at the top of the valence band. Combining these single particle states into exciton states yields the possible optical transitions observed in our experiments. Figure 1f shows the thus calculated absorption spectrum for both neutral (no holes or electrons) and singly charged QDs (1 electron or 1 hole). In the charged cases, additional intraband absorption occurs at longer wavelengths, especially involving intraband transitions of holes. The 4- and 2-fold degeneracy of the CB1 and VB1 states lead to an 8-fold degenerate lowest energy exciton – denoted by X_1. The combination of CB1 and VB2 states lead to a second exciton, X_2, with a similar 8-fold degeneracy, separated from X_1 by 54 meV in this calculation. We note that this energy difference strongly exceeds the typical phonon energies in HgTe (17 meV)[27], possibly rendering relaxation between these states slow. Importantly, the oscillator strength of the X2 transitions is about 10 times larger than that of the X1 transition (see Figure 1f), making that X2 dominates the absorption spectrum. Qualitatively similar results are obtained for tetrahedral nanocrystals (see Extended Data), which indicates that this basic picture of the level structure can be used to interpret experimental results on an ensemble of HgTe QDs with different shapes.

(964 words)

Broadband transient absorption spectroscopy

We analyzed optical gain in solution dispersed colloidal HgTe QDs using broadband transient absorption (TA) spectroscopy. This involved the excitation of a QD ensemble using a 200 fs laser pulse at 700 nm, followed by probing the change in absorbance $\Delta A = A - A_0$ (A: actual absorbance, A_0: absorbance in absence of pump pulse) as a function of wavelength and pump-probe temporal delay (see Methods Section for details). Note that the absorbance A is related to the absorption coefficient α through the cuvette length L: $A_i = \alpha_i L$. TA measurements are typically represented

using either the normalized absorption change ($\Delta A/A_0$) or the non-linear absorbance $A = \Delta A + A_0$, the more useful quantity when evaluating amplification. Bleaching (i.e. reduction) of the absorption, either through state-filling or spectral shifts corresponds to $\Delta A < 0$, while photo-induced absorption, either through intraband absorption[28,29] or spectral shifts corresponds to $\Delta A > 0$. Note that the occurrence of optical gain at a given wavelength is evidenced by $\Delta A < -A_0$ or, equivalently, a negative non-linear absorbance $A < 0$ at that wavelength. In that case, the sample emits more photons than it absorbs, *i.e.*, stimulated emission dominates over absorption.

A 2D TA image is shown in Figure 2, obtained after a 700 nm pump pulse that leads to an average number of absorbed photons per QD $\langle N \rangle$ of 0.1 (see Methods on determination of $\langle N \rangle$). The bleach of the first exciton transition, clearly visible around 1200 nm, narrows down and loses intensity in the first nanosecond after the pump pulse. In addition, the change in absorbance extends up to 1500 nm, a wavelength well beyond the first exciton transition. At these longer wavelengths, little dynamics is observed within the timeframe of the TA measurement. By comparing the difference $\delta(\Delta A) = \Delta A(2500\ \text{ps}) - \Delta A(5\ \text{ps})$ between spectral cuts at 5 ps (when carrier cooling is complete, see Supporting Information Figure 2) and 2.5 ns, it follows that especially the bleach at the blue side of the first exciton transition is reduced (green dotted line, Figure 2b). In view of the tight binding calculations, we attribute this change to the depletion of the high energy X2 manifold with large oscillator strength in favour of the lower energy X1, which has much lower oscillator strength. A detailed decomposition of the spectra shows that the X1-X2 splitting is 76 meV (see Supporting Information, figure 5), similar to the 54 meV splitting predicted by tight binding calculations. The X2-X1 relaxation happens on a 700 ps time-scale, a decay component also found in the time resolved photoluminescence traces (see Supporting Information, Figure 1). We thus conclude that the bleach of the first exciton transition reflects a relaxation of the holes between the V2 and V1 states.

(1368 words)

Nearly thresholdless gain

A more striking observation is the extension of the bleach spectrum up to 1500 nm. Figure 3a compares the corresponding bleach measured at a 2.5 ns delay for different pump fluences – increasing $\langle N \rangle$ from 0.006 to 0.3 – with the linear absorption and photoluminescence spectrum. It follows that at the long wavelength side a situation where $|\Delta A| > |A_0|$ is reached, *i.e.*, the sample amplifies the probe light, even for very low pump fluences. To make this observation more clear, Figure 3b plots the spectrum of the nonlinear absorbance $A = \Delta A + A_0$, again measured for a 2.5 ns delay, for different pump fluences. Note that this delay strongly exceeds the lifetime of multi-X, such that QDs contain a single exciton at the most. At low fluence ($\langle N \rangle < 0.006$), absorption dominates and $A > 0$ at all wavelengths. However, when increasing the fluence, α becomes negative in a small spectral region. Increasing the fluence further, yet remaining well below $\langle N \rangle = 1$, broadens this gain region from 1290 nm to 1510 nm, covering 3 technologically relevant transparency windows of commercial glass fibre (O,E and S-band, 1260 to 1530 nm, see also Figure 6). From Figure 3b, we can derive the threshold for stimulated emission as a function of wavelength. This is displayed in Figure 3c, which clearly shows that the threshold for optical gain is far below the single exciton occupation ($\langle N \rangle = 1$), dropping to 0.005 at

1500 nm. Note that this is, to the best of our knowledge, the lowest gain threshold ever reported for colloidal QDs, both in the visible and near-infrared part of the spectrum.

To confirm the single exciton character of the observed optical gain, we analyze the decay of the bleach signal, *i.e.*, the gain lifetime. If the gain effectively occurs in the single exciton regime, the decay should be on the order of the luminescent lifetime, *i.e.* 30-40 ns. Representative kinetic traces (at 1340 nm) are shown in Figure 3d. As we know from the previous analysis, increasing the fluence brings the differential absorbance beyond the gain threshold at populations far below $\langle N \rangle = 1$. More importantly however, the stimulated emission appears to be constant and persists longer than the measurable time window of the TA setup (2.5 ns). A fit to the apparently constant (in reality very slow) decay yields a lifetime of 34 ns, close to the measured 40 ns for the radiative single X decay. These findings confirm that the stimulated emission we observe is indeed due to singly excited QDs.

As can be seen in Figure 3d, faster decay components show up at higher pump fluence where multi-X states can be formed by multi-photon absorption. These multi-X decay on a 50 picosecond time-scale (see Supporting Information, Figure 2), which is typical for biexciton Auger recombination[30], quickly leaving behind a single excitation in the dots. Although ultrafast dynamics due to multi-X are present at higher pump fluence, we stress that the transient absorption does not drop below the gain threshold after the decay of the multi-X, confirming once more that multi-X are not required for optical gain. A very fast component (10 ps) is also superimposed on the multi-X decay (see Figure 3d), a feature which was also observed in studies relating to multiple-exciton generation[31]. In line with these authors, we attribute this component to fast non-radiative recombination in charged QDs that are formed at higher pump fluences[32]. A clear indication of this is found in the low fluence traces, where no ultrafast (10 ps) components are present. Moreover, refreshing the probed volume through stirring can reduce the relative weight of the ultrafast component, indicating that the recombination is non-intrinsic but due to formation of charged species in the volume under study (see Supporting Information, Figure 3).

With a degeneracy of 2 and 4 of the CB1 and VB1 states, population inversion at the bandgap transition will be reached at $\langle N \rangle = 4/3$ in the absence of size dispersion. When increasing the pump fluence up to these levels, an additional gain feature indeed appears at early time delays (10 ps, Figure 4a). This new gain band lies at the blue side of the low fluence gain and is lost at the long delay times where the low fluence gain still persists (2.5 ns, Figure 4a), with a detailed fitting yielding a lifetime of 93 ps at pumping levels of $\langle N \rangle = 1.2$. Moreover, its threshold $\langle N \rangle$ exceeds 1 at the shortest wavelengths where it occurs (Figure 4b). Based on this short lifetime and the threshold fluence, we attribute this additional gain band to multi-exciton gain across the X_1 transition.

Figure 4a shows that increasing the fluence beyond the single exciton level $\langle N \rangle = 1$ also introduces a rising absorptive background at the low energy side of the bleach spectrum. This reduces the stimulated emission and eventually leads to net absorption. We attribute the rising background to the presence of charged QDs that can result from, *e.g.*, Auger ionization of multi-excitons formed at higher pump fluences. As indicated by tight binding calculations (see Figure 1f), residual holes will in particular

give rise to a sizable additional absorption due to intraband transitions.[33,26] This excess amount of holes could also be correlated to the occurrence of the fast 10 ps component observed in the kinetic traces. Indeed, charged species will give rise to higher order recombination, *e.g.*, due to unbalanced excitons such as trions (single hole and exciton).

(2247 words)

HgTe QDs as effective 3-level systems

HgTe QDs exhibit optical gain below the one-exciton-per-QD limit as evidenced by their low fluence threshold for stimulated emission and the long gain lifetime. Moreover, the gain thresholds measured (see Figure 2d) appear to be limited only by residual loss channels such as intraband absorption at longer wavelengths[33]. This remarkable observation of nearly thresholdless gain in HgTe QDs implies that an emitting transition (i.e. with sufficient oscillator strength) is involved that has no counterpart in absorption at that specific wavelength, as is the case in specific 3-level and all 4-level systems. With QDs, this requirement is not met by the band gap transition. As a result, this transition only yields gain in the multi-X regime, unless more advanced core/shell nanocrystals exhibiting repulsive multi-X interactions are used[16]. These can bring the threshold slightly below the $\langle N \rangle = 1$ level, yet the almost thresholdless gain observed here remains out of reach also for these QDs. Thresholdless gain in QDs can be possible on the other hand if the gain transition involves states within the band gap. Indeed, a transition of a conduction-band electron to a gap state that is empty in unexcited QDs or of a valence-band hole to an occupied gap state that has no counterpart in absorption would make QDs nearly thresholdless effective 3-level systems. Although it is well-known that localized gap states can be deliberately introduced in QDs by doping[34], or may result from incomplete surface passivation, optical gain *via* such states has never been reported.

In the case of HgTe QDs, the assumption that the nearly thresholdless gain is related to a transition of a conduction-band electron to a shallow, empty gap state (see Figure 5a) leads to a concise picture in line with the experimental data. After non-resonant photo-excitation and the initial cooling, the two, 4-fold degenerate, hole states (VB1/VB2) and 2-fold degenerate electron states (CB) are occupied. Further cooling of the hole states imposes a slow decay on the interband transition, where the band gap bleach loses the contribution of the X_2 transition. At high fluence, short lived multi-X gain is observed across the interband transition. The presence of a shallow, empty gap state just above the VB1 state leads to the apparent extension of the band gap bleach to longer, sub-bandgap wavelengths. As it has no counterpart in the absorption spectrum of unexcited QDs, this transition can lead to the observed optical gain at fluences as low as 0.005 excitations per QD. The attribution of the sub-bandgap gain to a transition between CB1 and an empty gap state agrees with the observation that the dynamics of the VB2/VB1 hole relaxation is not observed in the gain dynamics (see Figure 5b). Within this model, the conduction-band electron has two parallel decay pathways. The gain coefficient of the gap-state transition (see next section) appears to be substantially lower than the absorption coefficient of the bandgap transition, making that no spontaneous emission is observed from this transition. However, it is sufficiently large to add power to the probe pulse by

stimulated emission without competing linear absorption, leading to nearly thresholdless optical gain.

To corroborate the link between optical gain and a gap-state related transition, we analysed the gain cross section of a given batch of HgTe QDs as a function of the number of sample purification cycles. Purification of colloidal QDs by addition of a non-solvent is typically used to separate the nanocrystals from residual reaction products (excess ligands, unreacted precursors, side products,…). It is however well known that repetitive washing reduces the photoluminescence efficiency by introducing surface states, a consequence of stripping passivating ligands from the nanocrystal surface[35]. As shown in Figure 5c, we find that the relative gain cross section – here determined as the ratio of the nonlinear absorption at 1340 nm of the sample analysed relative to a singly washed sample with equal concentration of QDs – increases with the number of washing steps. This is a strong indication that gain is indeed related to a transition involving a gap state at the QD surface, *e.g.*, created by an incomplete ligand coverage, rather than a transition intrinsic to HgTe QDs. Unless mentioned otherwise, the measurements presented here have been performed on doubly washed HgTe QDs.

(2931 words)

Performance of HgTe QD based gain media

The gain thresholds reported here for HgTe QDs are the lowest ever for optical amplification using colloidal materials – outperforming by 2 orders of magnitude the best Cd-based structures available in the visible range of the spectrum – and the gain lifetime exceeds that of multi-exciton gain by 3 orders of magnitude. Still, the question remains whether an effective 3-level system like HgTe QDs, where gain involves a transition to a gap state, can provide the modal threshold gain needed to achieve lasing when embedding the QDs in a feedback structure. To answer this question, Figure 6 shows the intrinsic gain coefficient g_i of 2 different batches of HgTe QDs, emitting at 1220 nm (analysed in the paper) and 1300 nm (analysed in the Extended Data). Actual gain coefficients are obtained by multiplying g_i with the QD volume fraction *f*, which amounts to 0.2 – 0.3 in a close packed film of dodecanethiol capped HgTe QDs (Figure 6, dashed lines). One sees that gain coefficients of 100 cm^{-1} are achieved across the entire telecommunication window (indicated with the standard pass bands O/E/S/C/L). These values correspond to material gains reported for competing technologies such as nanocrystalline silicon and epitaxial quantum dots[36] and would provide sufficient gain to allow for amplification of long-range surface plasmon polaritons (SPPs) for, *e.g.*, optical interconnects or SPP based lasers.[37] Moreover, the combination of gain threshold, gain lifetime and gain coefficients of 100 cm^{-1} make HgTe QDs a very promising gain material for integrated photonics, where in particular electrically pumped devices become feasible. Indeed, as mentioned by Wood et al. gain lifetimes of ca. 100 ns are required at sub-1 exciton population to achieve DC electrical pumping[23], specifications that are largely met by the colloidal HgTe QDs used in this work.

In summary, we observe nearly thresholdless optical amplification in HgTe QDs. This is attributed to a gap-state related transition that makes HgTe QDs an effective 3-level system, for which population inversion can be reached at pump fluences substantially

below the one-exciton-per-QD level. Although in this case, the gap states are related to the synthesis and processing methods used, the results show a new paradigm for light amplification using colloidal QDs. Rather than engineering the electronic properties (type 2 structures[16], Auger suppression[38]), one should focus on obtaining effective 3 level systems. When providing a sufficiently high gain coefficient, they can easily outperform the inherent 2 level systems obtained through the widely used electronic wavefunction engineering thanks to their low gain threshold and long gain lifetime. Further research must therefore address methods for the controlled formation of optimized gap states, either by surface engineering or impurity doping, a search that would profit from the support of theoretical calculations of level energies and transition oscillator strengths.

(3385 words)

Methods

Synthesis of HgTe nanocrystals

Colloidal QDs are synthesized by a modified procedure of Keuleyan et al[24] and Sungwoo et al[25]. As such, 270mg (1mmol) of HgCl2, 1.6 ml (6mmol) of dodecanethiol (DDT), 8ml of oleylamine (OLA) were mixed in a 25 ml flask and degassed under vacuum at 100°C for one hour and then the reaction mixture was placed under nitrogen while keeping the temperature at 60 °C. Next, 1ml of TOP-Te (1 mmol) was rapidly injected and QDs are allowed to grow at this temperature. After injection of the Te precursor, color of the reaction mixture darkened and appeared black in a few seconds. The reaction was quenched by injecting 10 ml of toluene and with a water bath. As obtained HgTe QDs were purified 2 times using toluene and methanol. Polystyrene (100.000 g/mol) was added to as obtained solutions to avoid clustering in solid films for TEM analysis.

Tight-binding calculations

The electronic structure and the optical properties of the HgTe nanocrystals have been studied theoretically following closely the methodology described by Delerue et al.[26] In a first step, the single-electron states are computed using a tight-binding model of HgTe. In a second step, the excitonic states $\Psi^{\mathrm{i}}_{\mathrm{exc}}$ are obtained using a Configuration Interaction (CI) method, i.e., they are expanded in a basis of Slater determinants built using the single-particle states obtained in tight-binding. The optical cross section of a single nanocrystal of dielectric constant $\varepsilon_{\mathrm{in}}$ embedded in a solvent of dielectric constant $\varepsilon_{\mathrm{out}}$ is given by

$$\sigma(\hbar\omega) = \frac{4\pi^2 e^2 F^2}{cn} \sum_i \omega_i \left| \left\langle 0 \right| \sum_n \mathbf{e}.\mathbf{r}_n \left| \Psi^{\mathrm{i}}_{\mathrm{exc}} \right\rangle \right|^2 L\,(\hbar\omega - \hbar\omega_i),$$

where $\hbar\omega$ is the photon energy, $\hbar\omega_i$ is the energy of the excitonic state $\Psi^{\mathrm{i}}_{\mathrm{exc}}$, $\mathbf{e}$ is the polarization vector, $n = \sqrt{\varepsilon_{\mathrm{out}}}$, $F = 3\varepsilon_{\mathrm{out}}/(\varepsilon_{\mathrm{in}} + 2\varepsilon_{\mathrm{out}})$ is the local-field factor. $\left\langle 0 \right| \sum_n \mathbf{e}.\mathbf{r}_n \left| \Psi^{\mathrm{i}}_{\mathrm{exc}} \right\rangle$ is the dipolar matrix element in which $\mathbf{r}_n$ is the position of the electron n. The function L is a Gaussian which describes the homogeneous/inhomogeneous broadening (here 35 meV) of the optical transitions. The photoluminescence lifetime τ is calculated using:

$$\frac{1}{\tau} = \frac{4e^2F^2n\sum_i p_i\omega_i^3\left|\langle 0|\sum_{n,\mathbf{e}}\mathbf{e}.\mathbf{r}_n\left|\Psi_{\mathrm{exc}}^{\mathrm{i}}\right\rangle\right|^2}{3c^3\hbar}$$

where p_i is the thermal population of the excitonic state $\Psi_{\mathrm{exc}}^{\mathrm{i}}$ at 300K. The effective dielectric constant is calculated in tight-binding as described in earlier work[39]. Basically, we calculate the screened electrostatic potential in a nanocrystal on which we apply a uniform (static) electric field. By fitting this potential using the expression derived from classical electrostatics theory, we deduce a value of $\varepsilon_{\mathrm{in}} = 6.8$ for a spherical nanocrystal of diameter 3.5 nm. We assume that the resulting local-field factor is the same in tetrahedral nanocrystals as in spherical nanocrystals with the same volume.

Linear Optical Properties

Lifetime measurements are carried out using a Hamamatsu near-infrared PMT in combination with a TCSPC (time-correlated single photon-couting) module (Edinburgh Instruments). Samples are prepared by diluting a solution of nanocrystals in tetrachloroethylene (Aldrich) to an optical density of 0.1 at the excitation wavelength of 650 nm.

Ultrafast pump-probe spectroscopy

Samples are pumped using 200 femtosecond pulses at 700 nm, created from the 1028 nm fundamental (Pharos SP, 6W, Light Conversion) through non-linear frequency mixing in an OPA (Orpheus, Light Conversion). Probe pulses are generated in a sapphire crystal using the 1028 nm fundamental. The pulses are delayed relative to the probe using a delay stage with maximum delay of 2.5 ns (Helios Spectrometer, Ultrafast Systems). The probe spectrum covers the VIS-NIR window from 450 nm up to 1620 nm. HgTe NCs are dispersed in a transparent solvent (tetrachloroethylene) to achieve optical densities of 0.1 at the first exciton transition. Samples are stirred during all measurements. No air-free sample handling was required as HgTe is , under our conditions, insensitive to oxidation. The average number of absorbed photons (or photo-generated excitons) at time zero $\langle N\rangle$ can be calculated as:

$$\langle N\rangle = J_{ph}\times\sigma_{700}\frac{1-e^{-\alpha_{700}L}}{\alpha_{700}L}$$

where J_{ph} is the photon flux in photons/cm^2 at 700 nm and σ_{700} is the absorption cross section of the nanocrystals at the pump wavelength of 700 nm. The additional factor corrects for variation of the pump fluence along the pump beam path length. σ_{700} is determined starting from $\mu_{i,400}$ (see section on intrinsic gain) as[40]:

$$\sigma_{700} = V_{QD}\times\mu_{i,400}\times\frac{A_{0,700}}{A_{0,400}}$$

where $A_{0,(400,700)}$ is the sample absorbance at 400 and 700 nm respectively and V_{QD} is the volume of the quantum dot. Note that the (relative) error on V_{QD} is 32% due to the size distribution obtained through TEM analysis. This allows us to determine the scaling factor between pump fluence (mW) and absorbed photons as 0.31 (±0.1) /mW. This translates into an error of 32% on all mentioned $\langle N\rangle$ values.

Calculation of intrinsic material gain

We can calculate the intrinsic gain based on the intrinsic absorption coefficient μ_i at high energies starting from bulk values for the (complex) dielectric function ($\varepsilon = \varepsilon_R + i\varepsilon_I$)[40]:

$$\mu_{i,400} = \frac{2\pi}{\lambda n_s} |f_{LF}|^2 \varepsilon_I = 4.84 \cdot 10^5 cm^{-1}$$

This theoretical value corresponds very well to the experimental value obtained by Lhuillier et al.[27] : $\frac{\mu_{i,415,Ref}}{\mu_{i,415,Theory}} = 0.87$. By measuring the linear absorption $A_{0,400}$ at 400 nm, we can determine the volume fraction f of nanocrystals in solution, since:

$$\mu_{i,400} (= 4.84 \cdot 10^5 cm^{-1}) = \frac{\ln(10)\, A_{0,400}}{fL}$$

From this, we calculate the intrinsic gain g_i plugging in the obtained f the non-linear absorption A (note that $A < 0$ in case of stimulated emission):

$$g_i = -\frac{\ln(10)\, A}{fL}$$

The intrinsic gain is the gain provided by a fictious material of 100% HgTe with the equivalent oscillator strength of a HgTe nanocrystal at that wavelength. Since in close –packed films the actual volume occupied by HgTe nanocrystals is smaller, we have to correct with the appropriate volume fraction (f = 0.2-0.3).

References

1. Yin, Y. & Alivisatos, P. Colloidal nanocrystal synthesis and the organic-inorganic interface. *Nature* **437,** 664–70 (2005).

2. Keuleyan, S., Lhuillier, E., Brajuskovic, V. & Guyot-Sionnest, P. Mid-infrared HgTe colloidal quantum dot photodetectors. *Nat. Photonics* **5,** 489–493 (2011).

3. Wang, X. *et al.* Tandem colloidal quantum dot solar cells employing a graded recombination layer. *Nat. Photonics* **5,** 480–484 (2011).

4. Kim, T. *et al.* Full-colour quantum dot displays fabricated by transfer printing. *Nat. Photonics* **5,** (2011).

5. Beard, M. C. *et al.* Comparing Multiple Exciton Generation in Quantum Dots To Impact Ionization in Bulk Semiconductors: Implications for Enhancement of Solar Energy Conversion. *Nano Lett.* 100726091447055 (2010). doi:10.1021/nl101490z

6. Galland, C. *et al.* Two types of luminescence blinking revealed by spectroelectrochemistry of single quantum dots. *Nature* **479,** 203–207 (2011).

7. De Geyter, B. *et al.* The Different Nature of Band Edge Absorption and Emission in Colloidal PbSe/CdSe Core/Shell Quantum Dots. *ACS Nano* **5,** 58–66 (2011).

8. Norris, D. J., Efros, A. L. & Erwin, S. C. Doped nanocrystals. *Science* **319,** 1776–9 (2008).

9. Aubert, T. *et al.* Homogeneously Alloyed CdSeS Quantum Dots: An Efficient Synthesis for Full Optical Tunability. *Chem. Mater.* **25,** 2388–2390 (2013).

10. Jenkins, A. Silicon Lasers: the Final Frontier. *Nat. Photonics* **1,** (2007).

11. Simply silicon. *Nat. Photonics* **4,** 491–491 (2010).

12. Franzo, G., Priolo, F., Coffa, S., Polman, A. & Carnera, A. Room-temperature electroluminescence from Er-doped crystalline Si. *Appl. Phys. Lett.* **64,** 2235–2237 (1994).

13. Daldosso, N. *et al.* Erbium and Silicon nanocrystals for light amplification. *LEOS 2007 - IEEE Lasers Electro-Optics Soc. Annu. Meet. Conf. Proc.* **2008,** 933–934 (2007).

14. Geiger, R. *et al.* Analysis of enhanced light emission from highly strained germanium microbridges. *Nat. Photonics* **7,** 466–472 (2013).

15. Klimov, V. I. Optical Gain and Stimulated Emission in Nanocrystal Quantum Dots. *Science (80-.).* **290,** 314–317 (2000).

16. Klimov, V. I. *et al.* Single-exciton optical gain in semiconductor nanocrystals. *Nature* **447,** 441–6 (2007).

17. Dang, C. *et al.* Red, green and blue lasing enabled by single-exciton gain in colloidal quantum dot films. *Nat. Nanotechnol.* **7,** 335–339 (2012).

18. Schaller, R. D., Petruska, M. a. & Klimov, V. I. Tunable Near-Infrared Optical Gain and Amplified Spontaneous Emission Using PbSe Nanocrystals. *J. Phys. Chem. B* **107,** 13765–13768 (2003).

19. Klimov, V. I. Quantization of Multiparticle Auger Rates in Semiconductor Quantum Dots. *Science (80-.).* **287,** 1011–1013 (2000).

20. Chen, Y. *et al.* Flexible distributed-feedback colloidal quantum dot laser. *Appl. Phys. Lett.* **99,** 241103 (2011).

21. García-Santamaría, F. *et al.* Suppressed auger recombination in “giant” nanocrystals boosts optical gain performance. *Nano Lett.* **9,** 3482–8 (2009).

22. Grivas, C. *et al.* Single-mode tunable laser emission in the single-exciton regime from colloidal nanocrystals. *Nat. Commun.* **4,** (2013).

23. Caruge, J. M., Halpert, J. E., Wood, V., Bulović, V. & Bawendi, M. G. Colloidal quantum-dot light-emitting diodes with metal-oxide charge transport layers. *Nat. Photonics* **2,** 247–250 (2008).

24. Keuleyan, S., Lhuillier, E. & Guyot-Sionnest, P. Synthesis of Colloidal HgTe Quantum Dots for Narrow Mid-IR Emission and Detection. *J. Am. Chem. Soc.* **133,** 16422–16424 (2011).

25. Kim, S. *et al.* Bandgap engineered monodisperse and stable mercury telluride quantum dots and their application for near-infrared photodetection. *J. Mater. Chem.* **21,** 15232–15236 (2011).

26. Allan, G. & Delerue, C. Tight-binding calculations of the optical properties of HgTe nanocrystals. *Phys. Rev. B* **86,** 1–6 (2012).

27. Lhuillier, E., Keuleyan, S. & Guyot-Sionnest, P. Optical properties of HgTe colloidal quantum dots. *Nanotechnology* **23,** 175705 (2012).

28. De Geyter, B. *et al.* Broadband and Picosecond Intraband Absorption in Lead-Based Colloidal Quantum Dots. *ACS Nano* **6,** 6067–6074 (2012).

29. Malko, a. V., Mikhailovsky, a. a., Petruska, M. a., Hollingsworth, J. a. & Klimov, V. I. Interplay between Optical Gain and Photoinduced Absorption in CdSe Nanocrystals. *J. Phys. Chem. B* **108,** 5250–5255 (2004).

30. Al-otaify, A., Kershaw, S. V, Gupta, S., Rogach, A. L. & Allan, G. Multiple exciton generation and ultrafast exciton dynamics in HgTe colloidal quantum dots. *Phys. Chem. Chem. Phys.* **15,** 16864–16873 (2013).

31. Al-Otaify, A. *et al.* Multiple exciton generation and ultrafast exciton dynamics in HgTe colloidal quantum dots. *Phys. Chem. Chem. Phys.* **15,** 16864–16873 (2013).

32. Allan, G. & Delerue, C. Fast relaxation of hot carriers by impact ionization in semiconductor nanocrystals: Role of defects. *Phys. Rev. B* **79,** 1–5 (2009).

33. Liu, H., Keuleyan, S. & Guyot-Sionnest, P. n- and p-Type HgTe Quantum Dot Films. *J. Phys. Chem. C* **116,** 1344–1349 (2012).

34. Viswanatha, R., Brovelli, S., Pandey, A., Crooker, S. a & Klimov, V. I. Copper-doped inverted core/shell nanocrystals with "permanent" optically active holes. *Nano Lett.* **11,** 4753–4758 (2011).

35. Hassinen, A. *et al.* Short-chain alcohols strip X-type ligands and quench the luminescence of PbSe and CdSe quantum dots, acetonitrile does not. *J. Am. Chem. Soc.* **134,** 20705–12 (2012).

36. Pavesi, L., Dal Negro, L., Mazzoleni, C., Franzò, G. & Priolo, F. Optical gain in silicon nanocrystals. *Nature* **408,** 440–4 (2000).

37. Berini, P. & De Leon, I. Surface plasmon–polariton amplifiers and lasers. *Nat. Photonics* **6,** 16–24 (2011).

38. García-santamaría, F. *et al.* Breakdown of Volume Scaling in Auger Recombination in CdSe / CdS Heteronanocrystals : The Role of the Core-Shell Interface. *Nano Lett.* (2011).

39. Delerue, C., Lannoo, M. & Allan, G. Concept of dielectric constant for nanosized systems. *Phys. Rev. B* **68,** 115411 (2003).

40. Hens, Z. & Moreels, I. Light Absorption by Colloidal Semiconductor Quantum Dots. *J. Mater. Chem.* **22,** 10406–10415 (2012).

Additional Information

Supplementary Information is linked to the online version of the paper at www.nature.com/nature

Acknowledgements
This research is funded by Ghent University (Special Research Fund), the FWO-Vlaanderen (G.0760.12, G.0794.10), BelSPo (IAP 7.35, photonics@be), EU-FP7 (Navolchi) and ERC-ULPICC.
S. Flamée is acknowledged for TEM imaging of the nanocrystals and R. Van Deun for the use of the steady-state and time-resolved photoluminescence setup.

Author Information
P. Geiregat carried out the steady state and time-resolved photoluminescence and ultrafast experiments, analysed the data, aided in theory development and wrote the manuscript.
A.J. Houtepen supervised the experiments, aided in theory discussions and wrote the manuscript.
F.C. Grozema provided support for the ultrafast spectroscopy.
L.K. Sagar synthesized the HgTe nanocrystals and performed structural characterization (TEM,XRD).
C. Delerue and G. Allan carried out the tight-binding simulations and aided in the theory development.
D. Van Thourhout aided in theory discussions and supervised the research.
Z. Hens initiated and supervised the research, aided in the theory development and wrote the manuscript.

No competing financial interests
Correspondence and requests should be addressed to Zeger.Hens@ugent.be

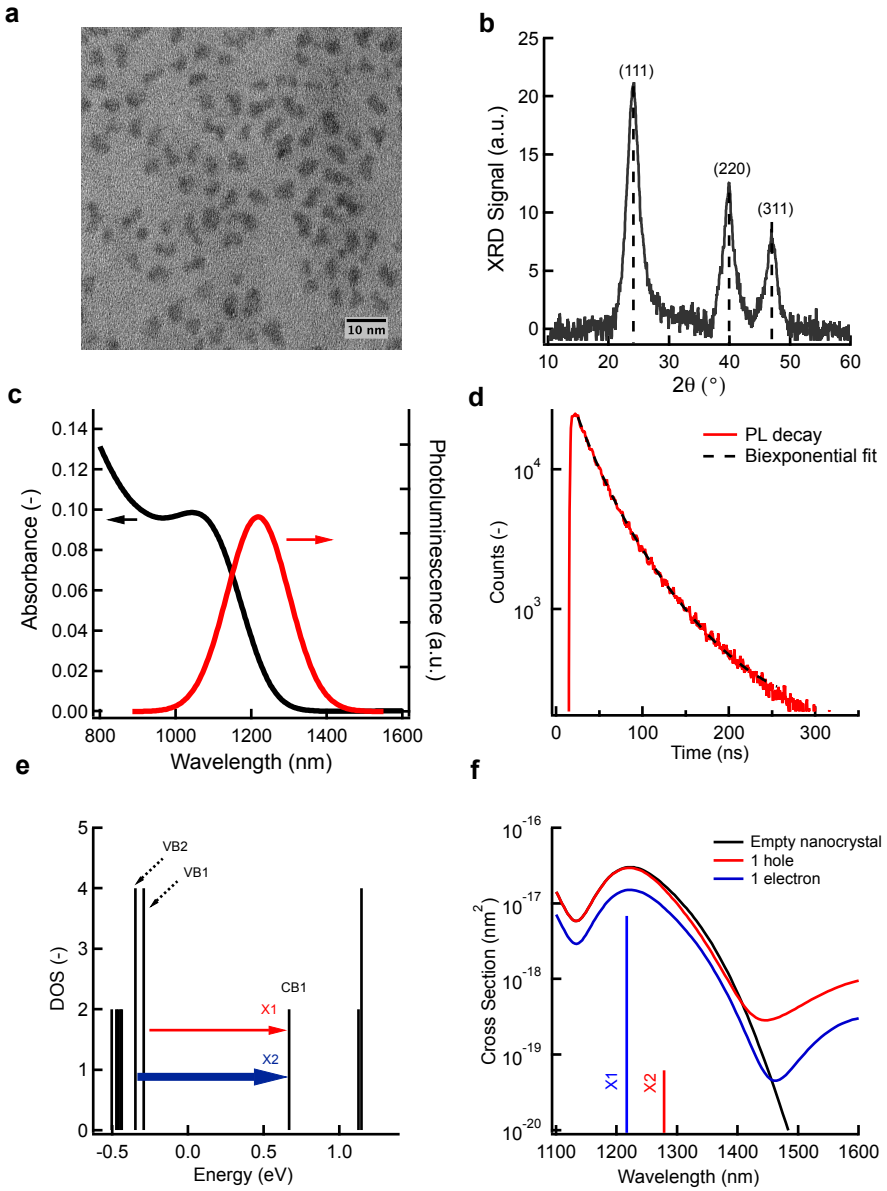

Figure 1: Structural and linear optical properties of HgTe nanocrystals (a) HR-TEM (High Resolution Transmission Electron Microscope) image of 3.5 ± 0.3 nm dodecane-thiol capped HgTe nanocrystals (b) XRD (X-Ray Diffraction) confirms zinc-blende crystallinity. Dashed lines indicate positions of the bulk HgTe diffraction pattern (c) Absorbance and emission of HgTe nanocrystals suspended in TCE as used in the TA experiments. (d) Photoluminescence (PL) decay of single exciton after 700 nm photoexcitation. A biexponential fit yields two distinct lifetimes: 35 (± 1.2) ns and 75 (± 3.2) ns (e) Density of States (DOS) of a spherical 3.5 nm HgTe nanocrystal calculated using tight-binding (f) Calculation of optical absorption spectra of an empty (no electron/hole) 3.5 nm HgTe nanocrystal based on DOS of figure 1.e. (solid black line). Also shown is the absorption when the crystal is charged with either 1 electron (solid blue line) or 1 hole (solid red line). The calculated exciton states X1 and X2 are also indicated with their relative oscillator strengths.

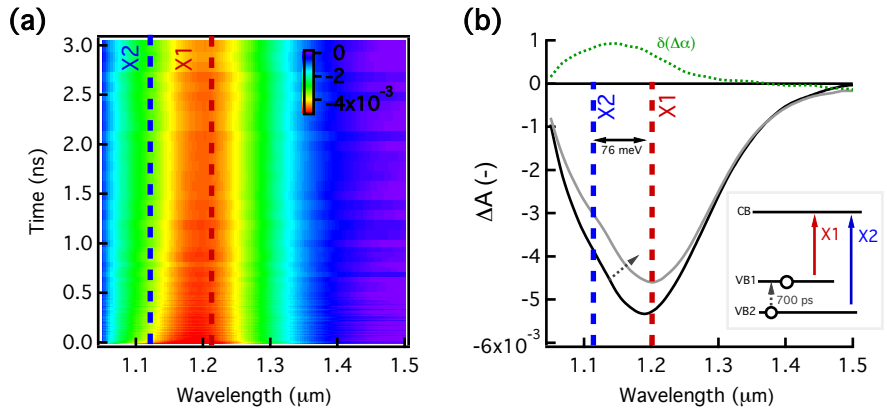

Figure 2: Two dimensional plot of ΔA, both as function of wavelength and time (a) Broadband image showing the broad bleach ($\Delta A < 0$) obtained after 700 photo-excitation at $t = 0$ with average number of absorbed photons per nanocrystal $\langle N \rangle = 0.1$. The band edge features X1 and X2 as predicted by the tight binding calculations (see Figure 1e) are added for comparison. (b) Taking spectral cuts at 5 (solid black line) and 2500 ps (solid grey line) shows the fine structure relaxation within the HgTe band edge, i.e. holes spread from VB2 to VB1 with a 700 ps time constant.

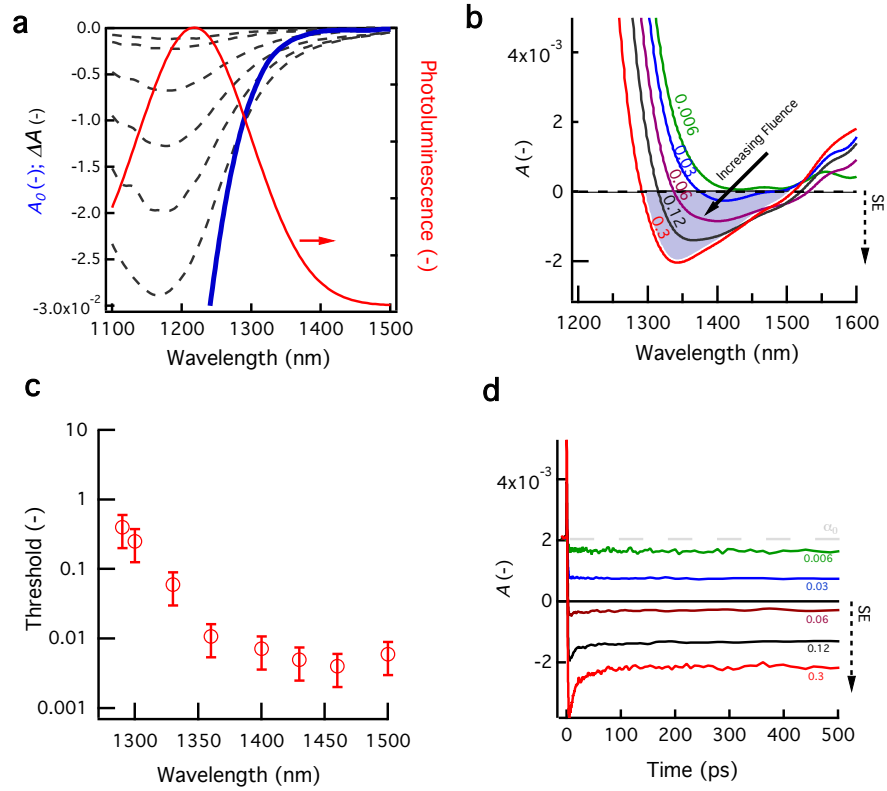

Figure 3: Analysis of fluence dependence (a) Fluence dependent difference spectra ΔA (grey dashed line), taken 2.5 ns after photo-excitation at 700 nm, plotted together with the linear absorption A_0 (solid blue line) and emission (solid red line). (b) Non-linear absorption spectra A, again taken 2.5 ns after photo-excitation. Stimulated emission (SE) corresponds to $A < 0$. The maximum gain bandwidth extends from 1310 to 1500 nm at sub-X fluence (<N>=0.3). (c) The wavelength dependence of the gain threshold as obtained from figure 3b (see text). (d) Kinetics of A at 1340 nm (gain maximum) for increasing fluence.

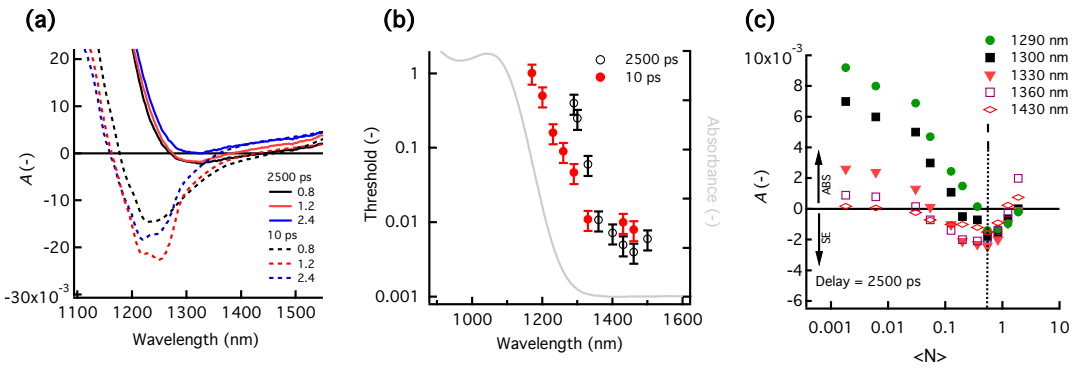

Figure 4: High fluence regime (a) Early time (10ps, dashed lines) and late-time (2500 ps, solid lines) non-linear absorbance spectra A for higher fluence (expressed as $\langle N \rangle$) (b) Wavelength dependence of gain threshold after 10 ps (red solid markers) and after 2500 ps (black empty markers), plotted together with linear absorbance (grey solid line) A_0 (c) Fluence dependence of non-linear absorbance A after 2500 ps for different probe wavelengths throughout the gain bandwidth. Note that optical gain corresponds to $A < 0$, i.e. stimulated emission (SE) dominates over absorption (ABS). We observe a loss of stimulated emission at higher pump fluence which we attribute to increased hole intraband absorption due to increased nanocrystal charging under high excitation rates.

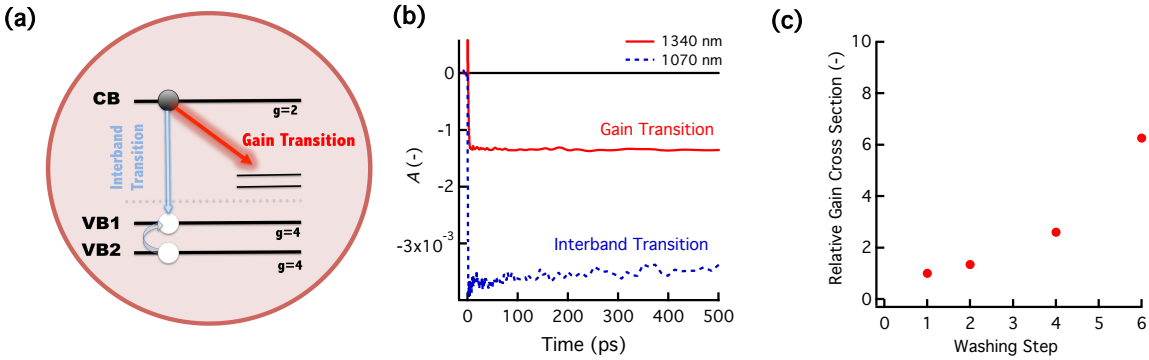

Figure 5: Thresholdless optical gain (a) Proposed model for thresholdless stimulated emission involving unoccupied shallow trap states close to the valence band. (b) Influence of hole X2-X1 dynamics on gain transition (black) and interband transition (red). (c) Increase of gain cross section (at 1340 nm) with subsequent washing steps, indicating that the shallow trap responsible for the thresholdless optical gain, is related to a surface defect (e.g. by insufficient surface passivation).

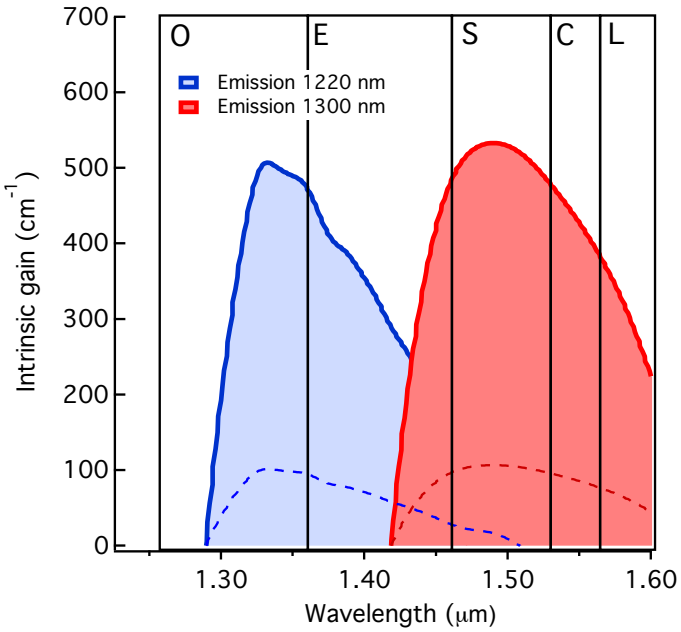

Figure 6: HgTe intrinsic material gain for two different samples emitting at 1220 nm (blue) and 1300 nm (red). The color-matching dashed lines indicate the volume-fraction corrected material gain. Note that the material gain provided by only 2 different sizes of HgTe covers the entire OESCL band with typical values over 100 cm^{-1}.

Supporting Information

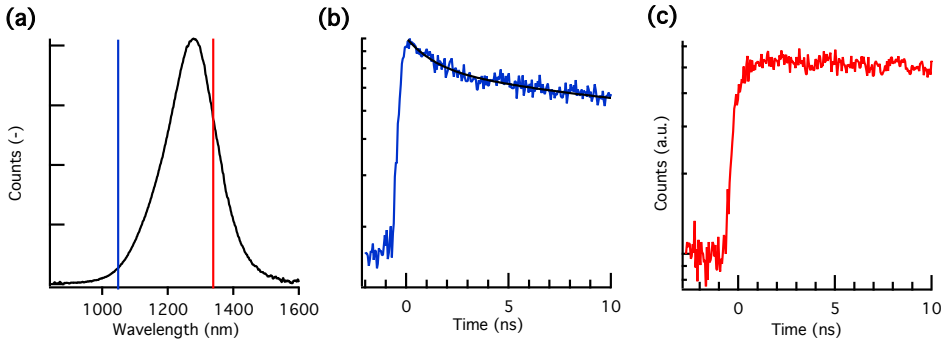

Figure S.1: Zoom of photoluminescence decay at blue and red side of emission spectrum (a) Steady state photoluminescence (PL) under 700 nm excitation. (b) PL decay at 1030 nm (blue line in (a)) and (c) 1370 nm (red line in (a)) for 700 nm excitaction (excitation pulse width = 0.1 ns). A bi-exponential fit in (b) yields a fast component lifetime of 1.1 ns, similar to the 0.7 ns component observed in the TA experiments (see main text).

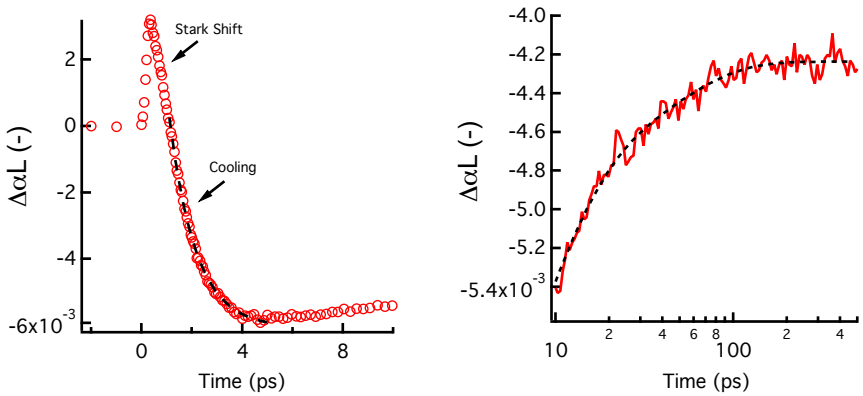

Figure S.2: Decay kinetic close-ups showing (left) the initial spectral shift (Stark Shift) leading to photo-induced absorption, followed by carrier cooling (1.5 ps time-constant) and (right) multi-X decay (Auger recombination time constant is 51 ps). A biexponential fit is needed to include the fast 10 ps higher order recombination (see text and discussion in SI).

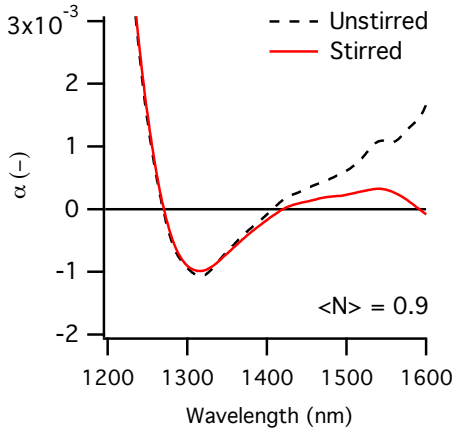

Figure S.3: Stirring of the solution influences the gain transition by reducing the hole-charging of the nanocrystals, thus alleviating additional intraband absorption.

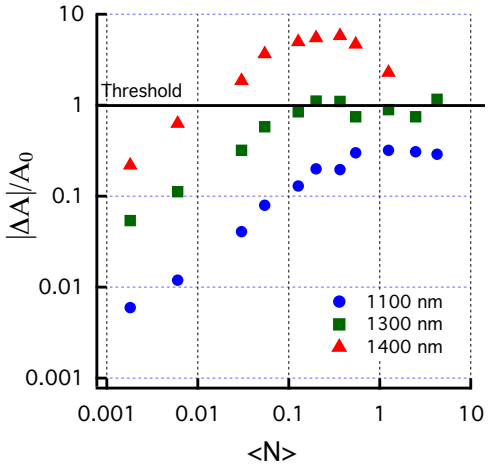

Figure S.4: Normalized bleach $\left|\frac{\Delta A}{A_0}\right|$ versus fluence for 3 different probe wavelengths. Note that optical gain corresponds to $\left|\frac{\Delta A}{A_0}\right| > 1$. In simple 3-level systems, $\left|\frac{\Delta A}{A_0}\right| < 2$ must hold. However, in our case, optical gain originates from a 4-level system making $\left|\frac{\Delta A}{A_0}\right| > 2$ possible.

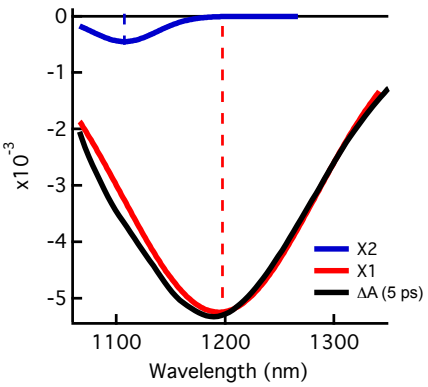

Figure S.5: Decomposition of early-time bleach spectrum in X1 and X2 contributions (see main text).

Discussion fast component

We attribute the fast (10-20 ps) decay component to unbalanced exciton recombination due to hole charging of the nanocrystals under high fluence excitation rates. This is based on 3 observations:

- Electron charging can only increase the gain cross section since it is the only carrier involved in the gain transition. Charging with holes will not increase the gain cross section, but leads instead to an increase of PA and a loss of gain. This is evidenced in the high fluence stirred/non-stirred comparison where stirring reduces the influence of hole charging by refreshing the excited volume.
- Hole intraband absorption is spectrally closer to the interband bleach and is much stronger (up to 1 order of magnitude) than electron intraband absorption (see tight binding calculations, figure 1.f)
- The weight of the fast decay component is smaller at the low energy side of the spectrum, involving only electron mediated transitions.

As such, holes are not involved in the gain transition but limit it by charging the crystals under high excitation rates, leading to a dominance of hole induced intraband absorption over stimulated emission. Electrons give rise to both interband bleach and trap-assisted stimulated emission. To alleviate the gain quenching at high excitation rate, a hole sink (e.g. by introducing charge transfer layers aimed at hole extraction) could be introduced.

Extended Data

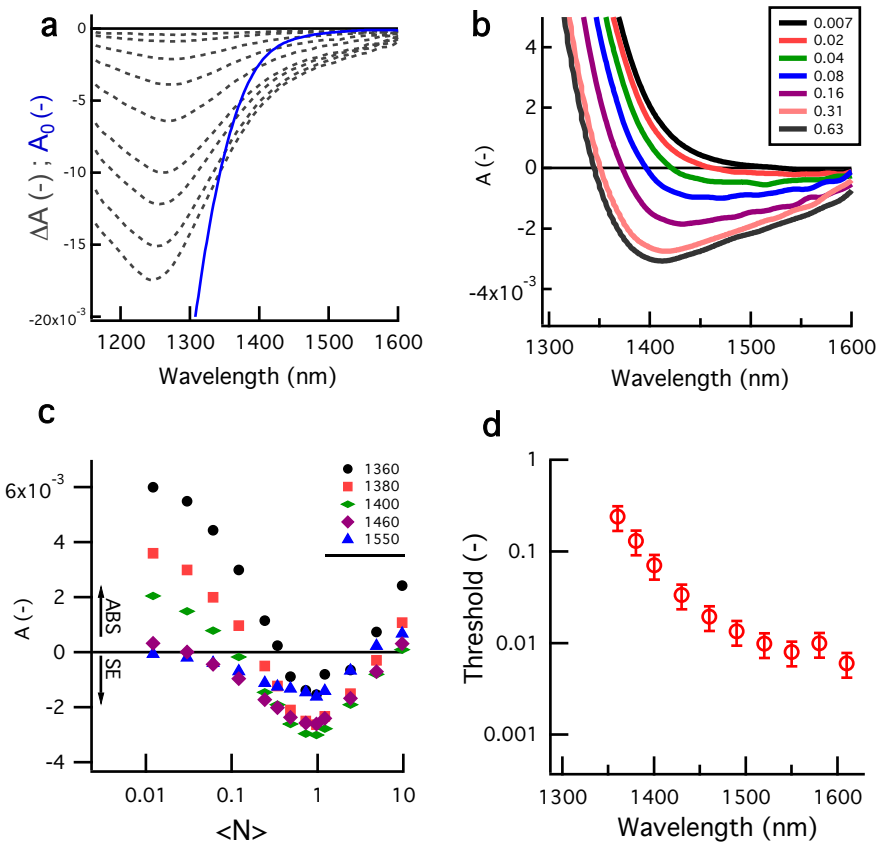

Figure X.1: Analysis of larger size (1300 nm emitting) HgTe nanocrystals providing gain from 1410 nm to beyond 1620 nm under similar thresholdless conditions as the 1220 nm emitting particles described in the main article.

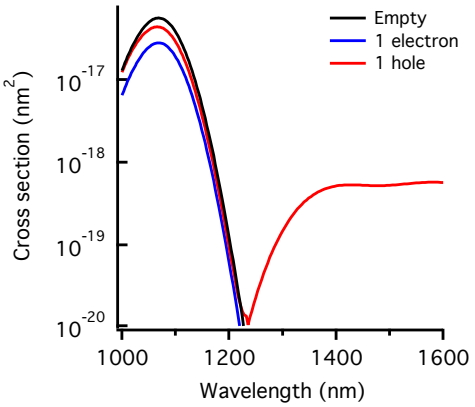

Figure X.2.: Cross Section of tetrahedral 3.5 nm HgTe for empty case and singly charged cases (1 electron or 1 hole) calculated using semi-empirical tight-binding approach (see Methods and main text).